

# LiDAL-Assisted RLNC-NOMA in OWC Systems

Ahmed A. Hassan, *Member, IEEE*, Ahmad Adnan Qidan, *Member, IEEE*, Taisir Elgorashi, *Member, IEEE*, and Jaafar Elmoghani, *Fellow, IEEE*

**Abstract**—Optical wireless communication (OWC) is envisioned as a key enabler for immersive indoor data transmission in future wireless communication networks. However, multi-user interference management arises as a challenge in dense indoor OWC systems composed of multiple optical access points (APs) serving multiple users. In this paper, we propose a novel dual-function OWC system for communication and localization. Non-orthogonal multiple access (NOMA) with random linear network coding (RLNC) is designed for data transmission, where NOMA allows the serving of multiple users simultaneously through controlling the power domain, and RLNC helps minimize errors that might occur during signal processing phase. This setup is assisted with a light detection and localization system (LiDAL) that can passively obtain spatio-temporal indoor information of user presence and location for dynamic-user grouping. The designed LiDAL system helps to improve the estimation of channel state information (CSI) in realistic indoor network scenarios, where the CSI of indoor users might be noisy and/or highly correlated. We evaluate the performance of NOMA combined with RLNC by analyzing the probability of successful decoding compared to conventional NOMA and orthogonal schemes. In addition, we derive the Cramer-Rao Lower Bound (CRLB) to evaluate the accuracy of location estimation. The results show that the proposed RLNC-NOMA improves the probability of successful decoding and the overall system performance. The results also show the high accuracy of the unbiased location estimator and its assistant in reducing the imperfection of CSI, leading to high overall system performance.

**Index Terms**—Optical wireless communication, NOMA, Network coding, RLNC, Localization.

## I. INTRODUCTION

Optical wireless communication (OWC) has emerged as a key technology for the next generation of indoor cellular systems (i.e., 6G), aiming to meet the increasing demands of massive device connectivity and ultra-low latency data services such as augmented and virtual reality (AR/VR) and real-time gaming [1]. OWC has received great interest from both academia and industry as it can enable multi-gigabit transmissions to indoor users by utilizing free-license optical spectrum and reusing existing illumination infrastructure [2], [3]. Furthermore, OWC systems can use different wavelengths (i.e., colors) to send information to multiple users, which would provide high spectral efficiency and security. In a typical OWC, the optical source, such as light-emitting diode (LED) or laser diode (LD) converts the data symbols into a form of optical signal, and the receiver equipped with a photo-diode detector (PD) converts the received optical power into electrical current that represents to the transmitted data symbols [4].

To satisfy the illumination requirements of a small indoor area, several optical sources (i.e., LEDs or LDs) are required. As a result, OWC systems would notably suffer from high levels of interference, especially in densely multi-user indoor

settings. Such interference poses a considerable degradation in the spectrum efficiency and strongly dictates the achievable user data rates within such scenarios. For this reason, managing user medium access becomes unavoidable [5], [6].

In this context, non-orthogonal multiple access (NOMA) has recently garnered widespread attention as a promising multiple access (MA) candidate for indoor OWC systems. Compared to conventional orthogonal multiple access (OMA) such as (i.e., TDMA, OFDMA, CDMA, ..., etc.), NOMA would significantly improve spectral efficiency and provide a balanced throughput and fairness trade-off [7]. Typical NOMA controls the power domain (PD-NOMA) to serve multiple users at different power levels of the same channel resource by applying the super positioning coding (SC) technique on transmitted users signals [8]. At the receiving end, successive interference cancellation (SIC) is employed to decode the signal of the intended user.

NOMA is applicable to uplink and downlink OWC transmissions. In downlink NOMA, users with weak channel gains are usually assigned more optical power than users with strong channel gains. In this case, users with weak channel gain can decode their signals while treating the signals of others as noise. In [9], [10] the performance of NOMA in OWC systems has been thoroughly investigated in various indoor environments and configurations. In which NOMA has shown that it can outperform traditional OMA in several key metrics such as the total ergodic sum rate and the outage probability. Like any technology, NOMA suffers from high data packet loss due to the imperfection of the SIC that results from residual noise during the separation process of the corresponding user signal.

Random linear network coding (RLNC) is introduced in [11] as a way to enhance transmission efficiency by combining data pieces (i.e., packets) with random coefficients, which can be independently chosen from a finite Galois field (GF). In RLNC, the coded packets can be transmitted instead of original packets, then users decode the corresponding original data packets using, for instance, a Gauss-Jordan elimination process. In fact, RLNC can efficiently improve system capacity and reduce the number of retransmissions. Moreover, RLNC does not require any code sequence synchronization and/or packet loss feedback [12] increasing robustness in various cluttered wireless environments. In OWC systems, several studies have proposed network coding to enhance transmission capacity, such as physical-layer network coding (PNC) [13] and relay-based network coding [14], [15]. For NOMA systems, RLNC is proposed to improve the packet success probability and the packet delay in RF- and OWC-based multicast networks as reported in [16] and [17], respectively.

In the last decade, most of the research in indoor NOMA-

based systems has considered channel state information (CSI) an intuitive parameter for user grouping and ranking, power allocation, and signal encoding/decoding. CSI has been evaluated under the assumption that the wireless channel conditions remain constant for a given time unit or varies independently following a composition of probabilistic models, i.e. Rayleigh and exponential distributions [10], [18]. However, utilizing location-based information in NOMA-based indoor systems did not receive the same attention as the CSI parameter, and that can be due to three main factors: low RF-based indoor positioning accuracy, induced signal processing overhead, and increased integration complexity [19]. Therefore, adopting native object detection and localization capabilities within OWC systems and incorporating prior knowledge of user location information would improve NOMA-based OWC system efficiency. This approach enables optimized user access to resources and minimizes system design overhead, especially in indoor scenarios characterized by rapid channel fluctuation and high levels of interference [20].

Various studies considered enabling the visible light positioning (VLP) in OWC systems. The majority of the VLP techniques and mathematical methods addressed in the literature can be categorized into four main types: RSS-based methods (i.e., trilateration, proximity, fingerprinting), time-based methods (i.e., TOA, TDOA, PDOA) [21], [22] and angulation methods (i.e., AOA, AOD), [22], [23] or hybrid methods [24]. In addition, VLP systems can be classified according to receiver type: non-imaging receivers (i.e., PD and angle diversity receiver (ADR)) [25], and imaging receivers (i.e., camera) [26].

For object detection, several mechanisms for object detection and recognition are proposed, such as infrared (IR) [27], laser radar (LADAR) [28], and visible light radar (LIDAR) [26]. These mechanisms can coexist in OWC systems to enable various capabilities, such as adaptive blockage avoidance and efficient resource management. In addition to that, several modified optical modulation schemes, such as PSS-PPM [29] and IM-OFDM [30], have recently been proposed to simultaneously accommodate both detection and communication functions in one system.

The studies in [31], [32], demonstrated that the aforementioned VLP techniques can achieve high localization accuracy (i.e. in centimeters) within ideal indoor OWC systems. However, limited research has considered both the detection and localization of indoor objects (i.e., furniture, surfaces,... etc.) as well as user-associated properties such as skin colors, worn clothes, and nomadic behaviors in realistic indoor OWC systems. Therefore, a light detection and localization system (LiDAL) was proposed in [33] to effectively use optical signals that are reflected from opaque objects and are captured by a non-imaging PD type receiver that monitors the change of light intensity in the space-time domain. The LiDAL system can passively obtain spatio-temporal indoor information of user presence and location.

In this work, we propose a novel dual-function OWC system. It features a multi-user NOMA with RLNC to enhance system capacity and mitigate errors that occur during signal processing in NOMA. This setup is assisted with

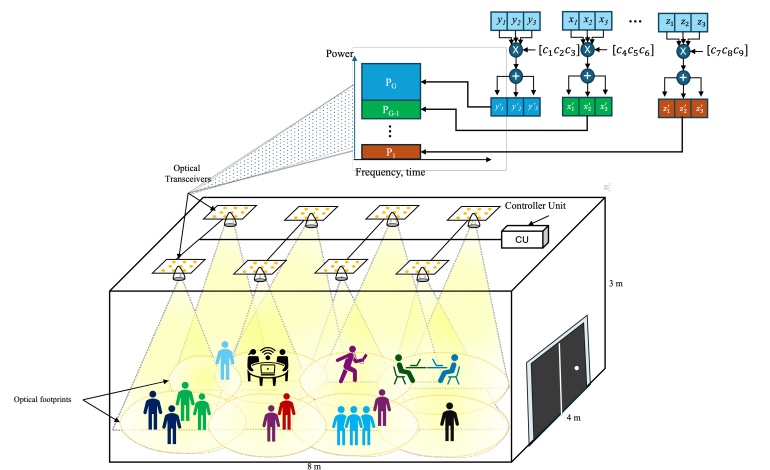


Fig. 1. LiDAL-assisted RLNC-NOMA system model

a multiple-input-multiple-output (MIMO) LiDAL system for user grouping. This localization system helps to improve the CSI estimation in a realistic scenario, where the CSI of indoor users might be noisy and/or highly correlated.

We evaluated the performance of NOMA combined with RLNC by analyzing the probability of successful decoding compared to conventional NOMA and OMA methods. In addition, we evaluated the MIMO-LiDAL localization probability and precision of the unbiased location estimator within the indoor environment considered.

The work is organized as follows. In Section II, we introduce the proposed system model which describes in detail the components of the RLNC-NOMA and MIMO-LiDAL systems. Section III analyze the system design and derive the unbiased location error estimator. Additionally, the LiDAL-assisted user grouping scheme is formulated using the user location information obtained. Section IV presents the simulation results and performance evaluation. Finally, Section V concludes our findings and remarks.

## II. SYSTEM MODEL

We consider an indoor OWC system model as illustrated in Fig.1, where multiple optical APs (i.e., transceivers) are installed on the ceiling to serve a large number of users in the communication plane. This system model combines two systems: RLNC-NOMA system and MIMO-LiDAL system, both are linked to a central control unit (i.e., controller). The description of both system models and their components is discussed in detail below.

### A. RLNC-NOMA System

A multi-user multiple input single output (MU-MISO) downlink configuration is considered. Each AP has a dual function transmitter  $Tx_k^L$ ,  $k = 1, 2, \dots, K$ , (i.e.,  $k$  optical footprint) that is equipped with a uniform array of LDs and is used for communication and localization (see Fig.1). A group-based NOMA is adopted to serve  $N$  communication users that are located and divided into at most  $K$  groups. Each user  $i$  (i.e.,  $i \in M_k$ ) associated with a transmitter  $Tx_k^L$

is equipped with a single PD that decodes the information symbols received by that user. For simplicity, we assume that the optical receivers of all system users are perpendicular to the communication plane and pointing toward the ceiling.

1) *RLNC-NOMA Channel Model*: In downlink NOMA scenario,  $Tx_k^L$  simultaneously transmits real and non-negative superimposed signals with different power levels to convey information to  $M_k$  users of the associated group  $k$ . Without loss of generality, the optical signals sent by optical AP  $k$  can be expressed by

$$\mathcal{S}_k = \mathcal{P}_t \sum_{i=1}^{M_k} \alpha_i s_i + I_{dc}, \quad \forall i \in M_k, k \in K \quad (1)$$

where  $s_i$  is the superimposed information signals,  $\alpha_i$  denotes the power allocation factor for user  $i$ .  $\mathcal{P}_t$  denotes the total transmission power, and  $I_{dc}$  is the direct current bias to ensure the positive intensity of the transmitted signals. To maintain non-negativity and control the eye safety of the transmitted optical signal, the following constraints should be satisfied, respectively.

$$\mathcal{P}_t \sum_{i=1}^{M_k} \alpha_i \leq I_{dc}, \quad (2)$$

and

$$\mathcal{P}_t \sum_{i=1}^{M_k} \alpha_i \leq A - I_{dc}, \quad (3)$$

where  $A$  is the maximum optical intensity of the corresponded optical AP  $k$ . For any PD type receiver, the signal received by user  $i$  from optical AP  $k$  is given by

$$\mathcal{Y}_i = \mathfrak{R}_i \tilde{h}_i \mathcal{P}_t \sum_{j=1}^{M_k} \alpha_j s_j + n_i, \quad \forall i \in M_k, k \in K \quad (4)$$

where  $\mathfrak{R}_i$  is the responsivity of PD,  $\tilde{h}_i$  denotes the channel gain coefficient,  $n_i$  is additive white Gaussian noise (AWGN) with zero mean and variance of  $\sigma_i^2 = (\sigma_{thr}^2 + \sigma_{shot}^2)$  due to the noise of the user receiver and the ambient noise at its location.

Under the assumption that each user's receiver points vertically toward the optical AP with narrow field-of-view (FOV) angle, we consider the LOS component (usually represents 90% of the overall received power) and neglect the diffuse components that are received due to reflections from the room walls and any other objects.

Therefore, the channel gain of the LOS component between the transmitter  $Tx_k^L$  of arbitrary optical AP  $k$  and the PD receiver of user  $i$  that belongs to  $M_k$  group of users is given by

$$\tilde{h}_i = \begin{cases} \frac{(m+1)A_{PD}}{2\pi\Lambda_i^{k2}} \cos^m(\phi_i) \cos(\psi_i) T_f(\psi_i) g_c(\psi_i), & 0 \leq \psi_i \leq \Psi_c \\ 0, & \text{otherwise} \end{cases} \quad (5)$$

where  $\phi_i$  and  $\psi_i$  denotes the irradiance and incidence angles between the transmitter  $Tx_k^L$  and the PD receiver of user  $i$ , respectively.  $\Lambda_i^k$  denotes the measured access distance between the location of user  $i$  and its associated optical AP  $k$  which corresponds in particular to the LOS distance between the PD receiver of user  $i$  and the transmitter  $Tx_k^L$  of the optical AP  $k$ ,  $\Psi_c$  represents the FOV angle of the PD receiver and  $A_{PD}$  denotes its physical area,  $m = -\frac{\ln 2}{\ln \cos \Phi_{1/2}}$  is the Lambertian index of  $Tx_k^L$  corresponding half-power semi-angle denoted by  $\Phi_{1/2}$ . Note that,  $T_f(\psi_i)$  and  $g_c(\psi_i)$  denote the optical filter gain of the PD receiver and the concentrator gain, respectively.

In this work, we assume that users are sorted in ascending order according to their access distances from the associated AP  $k$  (i.e.,  $\Lambda_1^k \leq \Lambda_2^k \leq \dots \leq \Lambda_{M_k}^k$ ). In this way, we have  $\alpha_1 \leq \alpha_2 \leq \dots \leq \alpha_{M_k}$  that satisfy the following NOMA conditions

$$\begin{cases} 0 \leq \alpha_i \leq 1, \\ \sum_{i=1}^{M_k} \alpha_i = 1. \end{cases} \quad \forall i \in M_k, k \in K \quad (6)$$

At the receiver side, the SIC decoder of user  $i$  decodes and subtracts the intended signals to all users at location  $X_m$  and have lower location order to the optical AP  $k$ , where ( $i+1 \leq m \leq M_k$ ). Moreover, the signals of all users with higher location order, where ( $1 \leq m \leq i$ ) are treated as noise. When SIC is performed on the superimposed information encoded using RLNC, and the signals intended for other users are subtracted, the received signal by the user  $i$  can be expressed as

$$\mathcal{Y}_i^* = \sum_{n=1}^f c_{in} b_{in} + n_i^*, \quad (7)$$

where  $c_{in}$  denotes a random chosen coding coefficient from the finite Galois field  $\text{GF}(2^8)$ ,  $b_{in}$  is the original packet of  $f$  packets transmitted over signal  $s_i$ , and  $n_i^*$  denotes a real-valued AWGN with zero mean and variance  $\sigma_*^2$  that represents the noise resulting from the imperfect SIC attributed to noisy and/or correlated user CSI.

Most of the literature contributions on NOMA are based on perfect knowledge of CSI (i.e.,  $\tilde{h}_i$ ) which is not ideal for designing practical MIMO NOMA-based systems. In other contributions, NOMA transmission with imperfect CSI (i.e.,  $\tilde{h}_i^*$ ) is considered instead of acquiring full channel CSI [10]. Furthermore, in distance-based NOMA systems, the user order may be suboptimal due to location estimation error and impaired channel conditions. However, exploiting additional location-based information using an integrated sensing and localization system (i.e., LiDAL) would efficiently capture the channel characteristics of users in a cluttered environment. Therefore, the location  $X_i$  of a user  $i$  can be characterised by its lower bound of location error  $B_i^L$  and its access distance  $\Lambda_i^k$  to the associated optical AP  $k$ . The corresponding imperfect CSI estimated error ( $\Delta \tilde{h}_i^* = \tilde{h}_i - \tilde{h}_i^*$ ) of user  $i$  at location  $X_i$  can be approximated by [34]

$$\Delta \tilde{h}_i^* \simeq \Delta_c \left( \frac{\eta^{m+1}}{(\Lambda_i^{k2} + B_i^{L2})^{\frac{m+3}{2}}} - \frac{\eta^{m+1}}{(\Lambda_i^{k2})^{\frac{m+3}{2}}} \right), \quad (8)$$

where  $\Delta_c = \frac{(m+1)A_{PD}}{2\pi} T_f(\psi) g_c(\psi)$ ,  $\eta$  denotes the height difference between a user  $i$  and the ceiling of the room

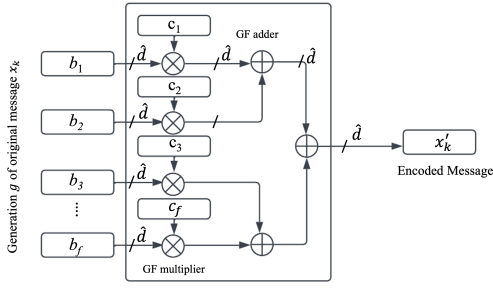


Fig. 2. RLNC-NOMA encoder design.

that is assumed to be fixed for all users in the considered indoor environment [33]. It is clear from the above that the imperfect CSI error is a function of two parameters, the estimated location error  $B_i^L$  and the measured access distance  $\Lambda_i^k$  of a user  $i$ . In fact, the CSI estimation error is inversely proportional to the estimated location error. Consequently, the RLNC-NOMA signal received by the user  $i$  can be easily derived from (7) and (8), and (4) can be rewritten in the following form

$$\mathcal{Y}_i = \mathfrak{R}_i(\tilde{h}_i^* + \Delta \tilde{h}_i^*) \mathcal{P}_t \sum_{n=1}^f \alpha_i c_{in} \cdot b_{in} + n'_i, \quad (9)$$

hence,  $n'_i = n_i^* + n_i$ .

2) *RLNC Encoder*: In optical AP, the RLNC encoder is utilized to encode the message packets  $\mathbf{X}_k$  (original packets) in the proposed system model. We assume progressive encoding [35] on a fixed-size buffer of original packets constituting a generation  $g$ , and each packet consists of a fixed length of  $\hat{d}$ -bytes. Initially, a basic partitioning and interleaving procedure [36] generates a matrix of byte symbols that represents a single generation of packets. This matrix is then multiplied by a vector of coding coefficients randomly chosen from  $\text{GF}(2^8)$ , followed by a GF addition process to produce elements or symbols in the same finite field, forming the encoded message packets  $\mathbf{X}'_k$  as illustrated in Fig.2.

3) *RLNC Decoder*: As soon as a sufficient number of linearly independent coded packets and the corresponding encoding coefficients are obtained after the optical signal separation process and demodulating the coded frames by the optical receiver, the RLNC decoder performs a progressive decoding on received coded packets and de-interleaves the decoded symbols to recover the original source packets as shown in Fig.3. The RLNC decoder can partially decode an original

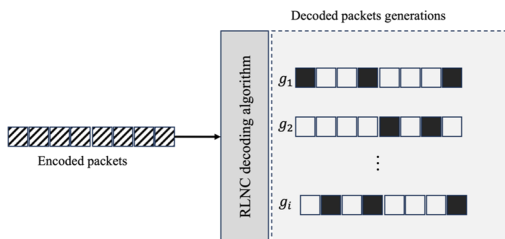


Fig. 3. RLNC-NOMA decoder design.

packet belonging to a generation before all coded packets of that generation  $g$  arrive. Therefore, a couple of decoding techniques are incorporated in the proposed RLNC decoder design, such as the LU decomposition algorithm, inversion of the encoding matrix, and Gauss-Jordan elimination [37]. These techniques are featured in receiver design to iteratively decode the original packets and enhance the decoding efficiency. In addition, a sliding window approach [36] is used to track previously decoded original packets that belong to a single generation  $g$ . In fact, the RLNC decoder does not require the received packets to be in order or need acknowledgment for the received coded packets. Moreover, the proposed decoding algorithm can be parallelized to optimize the performance and decrease the decoding stalls by implementing it on multi-core processors that are commercially available in current mobile devices.

### B. MIMO-LiDAL System

MIMO-LiDAL system consists of a set of LiDAL receivers (i.e., eight receivers) that are placed on the ceiling of the room and coupled to the OWC system transmitters (i.e., eight transmitters) as shown in Fig.1. Each LiDAL receiver is composed of three main components: optical receiver, target indicator, and sub-optimum receiver (SOR). First, the optical receiver consists of a single photodetector, a compound parabolic concentrator (CPC), and an optical filter. Second, the LiDAL target indicator that applies the cross-correlation method (CCM) [33], [38] on the received snapshots ( $S$ ) of measurements to distinguish users (targets) in the observed indoor environment. Finally, the SOR is composed of two elements: a zero-forcing equalizer (ZFE) to eliminate the effect of inter-time slots interference (ITI), and a threshold-based comparator for the target detection decision. In summary, the LiDAL receiver architecture is depicted in Fig.4. We assume that the MIMO-LiDAL system can utilize the same optical APs of the RLNC-NOMA communication system to generate detection and range optical pulses in pre-configured time slots  $T_s$  within a defined localization time window to avoid interference between detection and communication signals. Without loss of generality, we assume that a single arbitrary target user  $i$  is detected and located within the proposed MIMO-LiDAL system model at any given time.

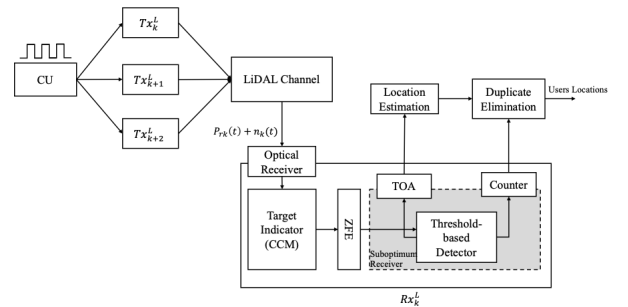


Fig. 4. MIMO-LiDAL receiver design.

As a result, the communication plane is divided into spatially overlapped optical footprints  $K$  as shown in Fig.1. The

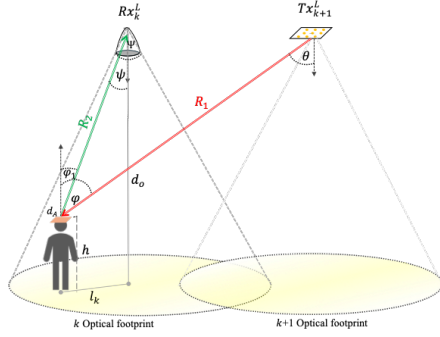


Fig. 5. Bistatic LiDAL configuration.

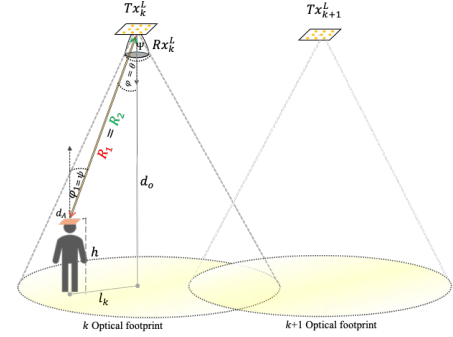


Fig. 6. Monostatic LiDAL configuration.

FOV angle of the LiDAL receivers (i.e., the optical footprints  $K$ ) is optimized to minimize the distance root mean square error (DRMSE) of the proposed MIMO-LiDAL system in the considered indoor environment. The minimum distinguishable distance between two arbitrary targets (localization resolution),  $\Delta R = 0.3m$  is maintained as in [33].

1) *LiDAL Configurations*: MIMO-LiDAL system has two possible transmitter and receiver configurations to detect and locate a user inside an optical footprint. First, bistatic LiDAL which refers to a spaced transmitter and receiver configuration as illustrated in Fig.5. Second, monostatic LiDAL which refers to a collocated transmitter-receiver (i.e., transceiver) configuration see Fig.6. In both configurations, we assume that the radiated optical signals from a transmitter and the reflected signals that obtained by a receiver follow a generalized Lambertian radiation pattern. Accordingly, the LOS optical power received from the reflected signal of a target user  $i$  by a bistatic LiDAL configuration is given by

$$P_{r_k}^{BLOS} = \begin{cases} \frac{(m+1)A_{PD}}{2\pi^2 R_1^2 R_2^2} P_t d_A \rho \cos^m(\theta) \cos(\psi) \times \\ \cos(\varphi) \cos(\varphi_1) T_f(\psi) g_c(\psi), & 0 < \psi < \Psi^L \\ 0, & \text{otherwise} \end{cases} \quad (10)$$

where  $P_t$  is the pulse power of the optical signal,  $A_{PD}$  is the PD area of the LiDAL receiver,  $d_A$  is the effective cross section of target user  $i$ ,  $\rho$  is the reflectivity factor of the user.  $R_1$  and  $R_2$  are respectively, the LOS range distance between the transmitter  $Tx_j^L$  and the target user  $i$ , and the LOS range distance between the target user  $i$  and the receiver  $Rx_k^L$  and  $k \neq j$ .  $\theta$  and  $\varphi_1$  devote respectively, the irradiance angle of the radiated signal of the transmitter  $Tx_j^L$  and the irradiance angle of the reflected signal of the target user  $i$ .  $\varphi$  and  $\psi$  are, respectively, the incidence angle of the optical signal transmitted to the target user  $i$ , and the incidence angle of the reflected signal of the target user  $i$  to the receiver  $Rx_k^L$ .  $T_f(\psi)$  and  $g_c(\psi)$  denote the optical filter and the optical concentrator gains, respectively.  $\Psi^L$  is FOV angle of the LiDAL receiver, and  $m$  denotes the Lambertian emission index. On the other hand, the optical power of the received reflected signal in a

monostatic LOS configuration is given by

$$P_{r_k}^{MLOS} = \begin{cases} \frac{(m+1)A_{PD}}{2\pi^2 R^4} P_t d_A \rho \cos^{m+3}(\psi) T_f(\psi) g_c(\psi), & 0 < \psi < \Psi^L \\ 0, & \text{otherwise} \end{cases} \quad (11)$$

where  $R$  (i.e.,  $R_1 = R_2$ ) is the LOS range distance between the transceiver ( $Tx_k^L$ - $Rx_k^L$ ) and a target user  $i$  within the optical footprint  $k$ . Note that,  $\psi$  represents both the irradiance and incidence angles where ( $\psi = \theta$  and  $\psi = \varphi_1$ ) of the transmitted optical signal and the reflected optical signal of target user  $i$  in the monostatic LiDAL configuration as shown in Fig.6.

2) *Localization method*: Time-of-arrival (TOA) technique is proposed in the MIMO-LiDAL system to estimate the location of users in the considered indoor environment. For an accurate localization of a user  $i$  inside an optical footprint  $k$ , a receiver  $Rx_k^L$  should obtain at least three range signals that are transmitted from three LiDAL transmitters  $Tx_j^L$ . In other words, for an arbitrary user  $i$  should be in the coverage of one monostatic LiDAL subsystem (i.e., optical footprint  $k$ ) and simultaneously ranged by at least two neighboring bistatic LiDAL subsystems ( $\forall j \in K^B, 2 \leq |K^B|, K^B \subset K$  and  $k \neq j$ ) as shown in Fig.7.

The time of arrival of a reflected pulse signal  $s(t)$  from target user  $i$  on a LiDAL receiver  $k$  within a time slot  $T_s$  can be written as

$$\mathcal{T}_i^k = \arg \max_{\tau} \left( \int_{-T_s}^{T_s} I_i^s P_{ri}(t - T_s + \tau) s(t) dt \right), \quad (12)$$

where  $P_{ri}$  is the received power of the reflected pulse signal,  $\tau$  is the time delay, and  $I_i^s$  is the CCM indicator of the presence of user  $i$  that occurred in a time interval  $T_s$  for consecutive measurements snapshots  $S$ . Thus,  $I_i^s$  can be defined as

$$I_i^s = \begin{cases} 0, & \text{if user } i \text{ is absent} \\ 1, & \text{if user } i \text{ is present} \end{cases} \quad (13)$$

The range of target user  $i$  lies inside a monostatic LiDAL (i.e., optical footprint  $k$ ) is given by.

$$R_i^k = \frac{\mathcal{T}_i^{k,j} c}{2}, \quad k \in K, k = j \quad (14)$$

where  $\mathcal{T}_i^{k,j}$  is the estimated TOA of the transmitter  $j$  signal and its reflection to a LiDAL receiver  $k$ , and  $c$  denotes the speed of light propagation. Therefore, the bistatic LiDAL range between transmitter  $j$  and user  $i$  can be derived as

$$R_i^j = \mathcal{T}_i^{k,j} c - R_i^k, \quad k, j \in K, k \neq j \quad (15)$$

Let us assume the location of target user  $i$  on the communication plane is defined by coordinates vector  $X_i = \begin{bmatrix} x_i \\ y_i \end{bmatrix}$  and it can be computed by the following range function.

$$R_k = \sqrt{(x_k - x_i)^2 + (y_k - y_i)^2}, \quad k \in K \quad (16)$$

where  $[x_k, y_k]^T$  is the location coordinates vector of the LiDAL transmitter  $Tx_k^L$  on the ceiling plane. By applying the least squares method, the location vector  $X_i$  of target user  $i$  can be estimated as an intersection of minimum three circles (i.e., optical footprints  $|K| \geq 3$ ), and it can be expressed in matrix notation as

$$\begin{bmatrix} \hat{x}_i \\ \hat{y}_i \end{bmatrix} = [A^T A]^{-1} A^T B, \quad (17)$$

where

$$A = \begin{bmatrix} x_k - x_1 & y_k - y_1 \\ \vdots & \vdots \\ x_K - x_1 & y_K - y_1 \end{bmatrix}, \quad (18)$$

and

$$B = \frac{1}{2} \begin{bmatrix} R_1^2 - R_k^2 - x_1^2 + x_k^2 - y_1^2 + y_k^2 \\ \vdots \\ R_1^2 - R_K^2 - x_1^2 + x_K^2 - y_1^2 + y_K^2 \end{bmatrix}, \quad (19)$$

for  $k = 2, \dots, K$ .

### III. SYSTEM DESIGN ANALYSIS

In this section, we discuss the integrated design functions of the RLNC-NOMA and MIMO-LiDAL systems, focusing primarily on the decoding success and the localization probability, respectively. Furthermore, an unbiased location error estimator is derived for the proposed MIMO-LiDAL system. A method to group users effectively using LiDAL-assisted technique is also proposed and analyzed.

#### A. RLNC-NOMA Decoding Success Probability

The total success probability of the proposed RLNC-NOMA and conventional NOMA schemes is derived to be evaluated for the system model considered. Generally, the total success probability is defined as the ratio of users who correctly recover all packets in a limited number of transmissions.

Initially, by applying the RLNC-NOMA transmission methodology, the achievable data rate  $\gamma_{k,i}$  for user  $i$  located in a group  $k$  is derived as follows [16].

$$\gamma_{k,i} = \begin{cases} B_w \log_2 \left( 1 + \frac{\mu_i \mathfrak{R}_i^2 h_i^2 \mathcal{P}_t^2 \alpha_i^2}{\mathfrak{R}_i^2 h_i^2 \mathcal{P}_t^2 \sum_{j=i+1}^{M_k} \alpha_j^2 + \sigma_i^2} \right) \leq \zeta, & 1 \leq i < M_k \\ B_w \log_2 \left( 1 + \frac{\mu_i \mathfrak{R}_i^2 h_i^2 \mathcal{P}_t^2 \alpha_i^2}{\sigma_i^2} \right) \leq \zeta, & i = M_k \end{cases} \quad (20)$$

where  $B_w$  denotes the PD receiver bandwidth,  $\zeta$  is the minimum NOMA throughput to capture a transmitted packet,  $\mathfrak{R}_k$  is the receiver PD responsivity of user  $i$ ,  $\mu_i$  is a constant to maintain the proportionality.

We assume that the total number of successive transmissions is denoted by  $V$ . Then, to derive the total probability of success, the probability of failure to transmit an arbitrary packet to a generic user  $i$  is denoted by  $\delta_{i,v}$  and given as [16].

$$\delta_{i,v} = 1 - \exp(-\varepsilon_i) \sum_{v=1}^V \frac{\varepsilon_i^{v-1}}{(v-1)!}, \quad \forall i \in M_k, k \in K \quad (21)$$

where  $v$  is the transmission index at which the successive transmission occurred.

Suppose that  $\varepsilon_{k,i}$  denotes the ratio of the optical channel gain to the power allocated to an arbitrary user  $i$  in a group  $k$  and be derived recursively as follows.

$$\varepsilon_{k,i} = \begin{cases} \frac{\Omega_{k,i}}{\mathcal{P}_t^2 \left( \alpha_i^2 - \alpha_{i+1}^2 (2^{\frac{\zeta}{B_w}} - 1) \right)}, & 1 \leq i < M_k \\ \frac{\Omega_{k,i}}{\mathcal{P}_t^2 \alpha_i^2}, & i = M_k \end{cases} \quad (22)$$

where  $\Omega_{k,i}$  is the channel gain of user  $i$  which belongs to group  $k$  which can be derived easily from (20). Note that  $\alpha_i^2 > \alpha_{i+1}^2 (2^{\frac{\zeta}{B_w}} - 1)$  is a necessary condition to satisfy the NOMA decoding order principle.

To compute the success probability for each user  $i$  within arbitrary group  $k$ , it is first assumed that the optical AP transmits each packet twice in the conventional NOMA scenario and four coded packets in the RLNC-based NOMA to maintain fairness. Furthermore, the binomial probability density function should satisfy the requirement that each user receives at least two packets in both scenarios. Consequently, the total success probabilities for the RLNC-NOMA ( $\hat{p}_s$ ) and the NOMA ( $p_s$ ) schemes in the  $v$ -th successive transmission are derived from [16], [39] and given respectively by

$$\hat{p}_s = \prod_{i=1}^{M_k} 1 - \left( \sum_{\lambda=0}^{f-1} \binom{\hat{\tau}}{\lambda} (\delta_{i,v})^{\hat{\tau}-\lambda} (1 - \delta_{i,v})^\lambda \right), \quad (23)$$

$$p_s = \prod_{i=1}^{M_k} (1 - \delta_{i,v})^f, \quad (24)$$

where  $f$  is the total number of packets in the frame (generation) and  $\hat{\tau}$  donates the total number of transmission attempts to all users of group  $k$  considered in the RLNC-based NOMA scenario. It is worth pointing out that  $v = 1$  in (23) since users are assumed to receive a linearly independent coded packet at any given time.

#### B. MIMO-LiDAL Localization Probability

In the proposed MIMO-LiDAL system, three unique LiDAL scans are required from adjacent transceivers to detect the target user  $i$  and estimate its location. Implicitly, the probability

of localizing users in the MIMO-LiDAL system is based on the independent detection probability of the monostatic LiDAL subsystem and the probability of the collaborating  $k$  bistatic LiDAL subsystems. Therefore, the probability of localizing target user  $i$  within overlapping optical footprints  $K$  can be derived as

$$P_i^L = P_D^M \prod_{k=2}^K P_D^B(k), \quad k \in K \quad (25)$$

where  $P_D^M$  is monostatic LiDAL detection probability of target user  $i$  and  $P_D^B$  is the detection probability of all adjacent  $k$ -bistatic LiDAL subsystems of the same target user. The monostatic LiDAL subsystem detection probability can be derived as [33]

$$P_D^M = \frac{1}{2} Q\left(\frac{D_{th}^M - \mu_M}{\sqrt{2}\sigma_M}\right). \quad (26)$$

The detection probability of an adjacent  $k$ -th bistatic LiDAL subsystem is given by [33]

$$P_D^B(k) = \frac{1}{2} Q\left(\frac{D_{th}^B(k) - \mu_B(k)}{\sqrt{2}\sigma_B(k)}\right), \quad (27)$$

where  $Q(\cdot)$  is the error function,  $\mu_M, \sigma_M$  respectively are the mean and variance of the received power in monostatic LiDAL subsystem.  $\mu_B$  and  $\sigma_B$  denote respectively, the mean and variance of the power received from the  $k$ -th bistatic subsystem.  $D_{th}^M$  and  $D_{th}^B$  denote respectively, the detection thresholds of monostatic and  $k$ -bistatic LiDAL subsystems. The detection threshold of both subsystems can be computed by [33]

$$D_{th} = \sqrt{\left(\frac{\mu^2}{(\beta_\sigma - 1)^2} + \frac{\mu^2}{\beta_\sigma - 1} + \frac{2\sigma^2}{\beta_\sigma - 1} (\ln \frac{\gamma_{FP}}{\gamma_{FA}} - \ln \frac{\hat{\sigma}_t}{\sigma})\right) - \frac{\mu}{\beta_\sigma - 1}}. \quad (28)$$

Thus,  $\mu$  and  $\sigma$ , respectively, are the mean and standard deviation of the received reflected signals in each respective LiDAL subsystem. Note that,

$$\sigma^2 = \hat{\sigma}_t^2 + \hat{\sigma}_s^2, \quad (29)$$

where  $\hat{\sigma}_s$  standard deviation the received reflected signals in noise.  $\hat{\sigma}_t = \sqrt{(\hat{\sigma}_{thr}^2 + \hat{\sigma}_{shot}^2)}$  denotes total of standard deviation of both thermal noise and shot noise components of an arbitrary LiDAL receiver [33].  $\beta_\sigma \geq 1$  represents the factor that measures the variance of the reflected signals due to the target coating effect (i.e., worn cloth materials and colors). This  $\beta_\sigma$  factor can be given by [33]

$$\beta_\sigma = \frac{\hat{\sigma}_s^2 + \hat{\sigma}_t^2}{\hat{\sigma}_t^2}. \quad (30)$$

Moreover,  $\frac{\gamma_{FP}}{\gamma_{FA}}$  is the LiDAL likelihood test-ratio threshold for SOR detection decision. knowing that  $\gamma_{FP}$  is the cost factor of missing a user presence, and  $\gamma_{FA}$  is the cost factor of falsely identifying the presence of a user in an indoor environment.

In our proposed MIMO-LiDAL system, we assume the cost of missing a user is high, then the test-ratio threshold should

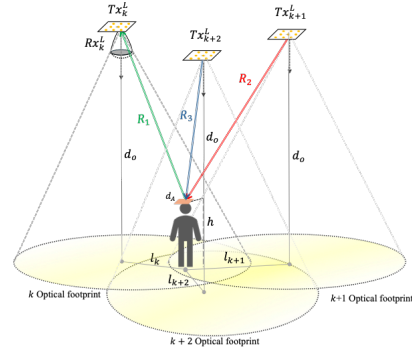


Fig. 7. MIMO-LiDAL localization system.

be set very low. Consequently, the LiDAL test-ratio threshold cost factors are set as  $\gamma_{FP} = 1$  and  $\gamma_{FA} = 100$  to minimize the probability of error in detecting and estimating the location of the user in the considered indoor environment [33].

### C. MIMO-LiDAL Cramer-Rao Lower Bound

The minimum error of arbitrary user location estimation in the MIMO-LiDAL system model can be analytically derived by the Cramer-Rao Lower Bound (CRLB) [40]. CRLB is known as the lower bound on the mean square error of the unbiased parameter estimator. However, the CRLB is widely used to theoretically evaluate the accuracy of location estimation using wireless technologies.

In this work, we derived CRLB to provide a baseline of the accuracy of the proposed localization method in the proposed LiDAL-assisted OWC system. The total LOS optical power received from user-reflected signals by the LiDAL receiver can be expressed by

$$Pr_{LOS}^{Total} = Pr_1^{MLOS} + \sum_{k=2}^K Pr_k^{BLOS} + \sum_{k=1}^K n_k, \quad \forall k \in K \quad (31)$$

where  $Pr^{MLOS}$  and  $Pr^{BLOS}$  represent the received LOS optical power from monostatic and  $k$ -bistatic subsystems, respectively.  $n_k$  denotes the AWGN of the LiDAL optical channel. Knowing that in (10),  $\cos(\theta_k) = \frac{(d_0 - h')}{R_k^2}$  for  $k = 2, \dots, K$  and in (11)  $\cos(\psi_1) = \frac{(d_0 - h')}{R_1^2}$  for  $k = 1$ . The range distance  $R_k$  in (16) can be rewritten as

$$R_k = \sqrt{l_k^2 + (d_0 - h')^2}, \quad \forall k \in K \quad (32)$$

where  $l_k$  is the distance between a projection of a transmitter  $Tx_k^L$  on the communication plane and target user  $i$ .  $d_0$  denotes the ceiling height of the room, and  $h'$  represents the vertical height of the cross section of target user  $i$ , as shown in Fig.7. Moreover, the optical power received from LOS in the equations of monostatic and  $k$ -bistatic subsystems can be reformulated, respectively, as

$$Pr_1^{MLOS} = \Delta_l \frac{\eta^{m+3}}{(l_1^2 + \eta^2)^{\frac{m+7}{2}}}, \quad k = 1 \quad (33)$$

and

$$Pr_k^{B_{LOS}} = \Delta_l \frac{\eta^{m+3}}{(l_1^2 + \eta^2)^2 (l_k^2 + \eta^2)^{\frac{m+3}{2}}}, \quad k = 2, \dots, K \quad (34)$$

where  $\Delta_l = P_t \frac{(m+1)A_{PD}}{2\pi^2} d_{AP} T_f(\psi) g_c(\psi)$ .

The total optical power of the LOS signals received by the LiDAL receiver can be written as a function of the Euclidean distance  $f(l_k)$  of a transmitter  $Tx_k^L$  and the location of target user  $i$ , and the height difference  $\eta$ . Accordingly, the first two terms in (31) can be denoted in a vector notation as

$$\mathbf{f}(\mathbf{l}) = \begin{bmatrix} f_1(l_1) \\ \vdots \\ f_k(l_k) \\ \vdots \\ f_K(l_K) \end{bmatrix}, \quad \forall k \in K \quad (35)$$

and the last noise term is denoted by

$$\mathbf{n} = \begin{bmatrix} n_1 \\ \vdots \\ n_k \\ \vdots \\ n_K \end{bmatrix}, \quad \forall k \in K \quad (36)$$

Subsequently, the first derivative of  $f(l)$  is given by

$$\frac{\partial \mathbf{f}(\mathbf{l})}{\partial \mathbf{l}^T} = \begin{bmatrix} \frac{\partial f_1(l_1)}{\partial l_1} & \dots & \frac{\partial f_1(l_1)}{\partial l_K} \\ \vdots & \ddots & \vdots \\ \frac{\partial f_K(l_K)}{\partial l_1} & \dots & \frac{\partial f_K(l_K)}{\partial l_K} \end{bmatrix}, \quad \forall k \in K \quad (37)$$

It is worth mentioning that  $\frac{\partial f_i(l_i)}{\partial l_j} = 0$  when  $i \neq j$ . Thus,  $\frac{\partial \mathbf{f}(\mathbf{l})}{\partial \mathbf{l}^T}$  is a diagonal matrix, and it can be written as

$$\frac{\partial \mathbf{f}(\mathbf{l})}{\partial \mathbf{l}^T} = -\Delta_l \text{diag} \begin{bmatrix} \frac{\Pi^M l_1}{(l_1^2 + \eta^2)^{\frac{m+9}{2}}} \\ \frac{\Pi^B l_2}{(l_1^2 + \eta^2)^2 (l_2^2 + \eta^2)^{\frac{m+5}{2}}} \\ \vdots \\ \frac{\Pi^B l_k}{(l_1^2 + \eta^2)^2 (l_k^2 + \eta^2)^{\frac{m+5}{2}}} \\ \vdots \\ \frac{\Pi^B l_K}{(l_1^2 + \eta^2)^2 (l_K^2 + \eta^2)^{\frac{m+5}{2}}} \end{bmatrix}^T, \quad \forall k \in K \quad (38)$$

where  $\Delta_l, \Pi^M = (m+7)\eta^{m+3}$ , and  $\Pi^B = (m+3)\eta^{m+3}$  are constants.

Let  $X_k^{tx} = \begin{bmatrix} x_k \\ y_k \end{bmatrix}$  is the location vector of LiDAL transmitter  $Tx_k^L$ . The distance between the projected location of LiDAL transmitter  $X_k^{tx}$  and the location of target user  $X_i$  on the communication plane can be computed by

$$\begin{cases} l_1^2 = (x_i - x_1)^2 + (y_i - y_1)^2, \\ \vdots \\ l_K^2 = (x_i - x_K)^2 + (y_i - y_K)^2. \end{cases} \quad \forall k \in K \quad (39)$$

Then, we have

$$\frac{\partial \mathbf{l}}{\partial \mathbf{X}^T} = \begin{bmatrix} \frac{\partial l_1}{\partial x_i} & \frac{\partial l_1}{\partial y_i} \\ \vdots & \vdots \\ \frac{\partial l_K}{\partial x_i} & \frac{\partial l_K}{\partial y_i} \end{bmatrix} = \begin{bmatrix} \frac{x_i - x_1}{l_1} & \frac{y_i - y_1}{l_1} \\ \vdots & \vdots \\ \frac{x_i - x_K}{l_K} & \frac{y_i - y_K}{l_K} \end{bmatrix}. \quad (40)$$

Accordingly, the CRLB of error of location estimation is given by

$$B^L(\mathbf{X}) = \left[ \left( \frac{\partial \mathbf{f}(\mathbf{l})}{\partial \mathbf{l}^T} \right)^T \mathbb{Q}^{-1} \left( \frac{\partial \mathbf{f}(\mathbf{l})}{\partial \mathbf{X}^T} \right) \right]^{-1}, \quad (41)$$

where  $\mathbb{Q} = E[\mathbf{n}\mathbf{n}^T]$  denotes the noise covariance matrix. By applying the chain rule  $\frac{\partial \mathbf{f}(\mathbf{l})}{\partial \mathbf{X}^T} = \frac{\partial \mathbf{f}(\mathbf{l})}{\partial \mathbf{l}^T} \frac{\partial \mathbf{l}}{\partial \mathbf{X}^T}$ , we obtain

$$\frac{\partial \mathbf{f}(\mathbf{l})}{\partial \mathbf{X}^T} = -\Delta_l \begin{bmatrix} \frac{\Pi^M l_1 (x_i - x_1)}{(l_1^2 + \eta^2)^{\frac{m+9}{2}}} & \frac{\Pi^M l_1 (y_i - y_1)}{(l_1^2 + \eta^2)^{\frac{m+9}{2}}} \\ \frac{\Pi^B l_2 (x_i - x_2)}{(l_1^2 + \eta^2)^2 (l_2^2 + \eta^2)^{\frac{m+5}{2}}} & \frac{\Pi^B l_2 (y_i - y_2)}{(l_1^2 + \eta^2)^2 (l_2^2 + \eta^2)^{\frac{m+5}{2}}} \\ \vdots & \vdots \\ \frac{\Pi^B l_k (x_i - x_k)}{(l_1^2 + \eta^2)^2 (l_k^2 + \eta^2)^{\frac{m+5}{2}}} & \frac{\Pi^B l_k (y_i - y_k)}{(l_1^2 + \eta^2)^2 (l_k^2 + \eta^2)^{\frac{m+5}{2}}} \\ \vdots & \vdots \\ \frac{\Pi^B l_K (x_i - x_K)}{(l_1^2 + \eta^2)^2 (l_K^2 + \eta^2)^{\frac{m+5}{2}}} & \frac{\Pi^B l_K (y_i - y_K)}{(l_1^2 + \eta^2)^2 (l_K^2 + \eta^2)^{\frac{m+5}{2}}} \end{bmatrix}. \quad (42)$$

The CRLB of location estimation error in our proposed MIMO-LiDAL system can be obtained by substituting both equations (38) and (42) in  $B^L(\mathbf{X})$ . In particular, CRLB estimated parameter is utilized to enable the power allocation of the integrated RLNC-NOMA communication system that serves multiple users within the realistic indoor environment considered.

#### D. LiDAL-assisted User Grouping Scheme

To increase the throughput of users with poor channel gains (low location orders), it is beneficial to pair them with users with high channel gains (high location orders). The reason is that users with high channel gains can still achieve a higher data rate even if they have been assigned to lower power levels while making a large portion of the optical power of AP  $k$  available to users with weak channel gains.

Consequently, we propose a LiDAL-based suboptimal user grouping algorithm that consists of three main operations: determine the adjacent APs ( $\forall k \in K^*$ ,  $K^* \subseteq K$ ) that have the minimum Euclidean distance  $f_i(k)$  to the estimated locations of OWC users on the communication plane. Then, sorting user locations according to a CRLB location error estimate  $B_k^L(X_i)$  and dividing them into two classes: Class I consists of users with low estimated location errors, and class II consists of users with high estimated location errors. Next, sort these users according to their access distance  $\Lambda_i^k$  between their locations (estimated locations) and the potential adjacent APs. Finally, apply the D-NLUPA method [41] to pair users from both classes based on their largest difference in access distances  $\Lambda_i^k$ , to be assigned to a single adjacent optical AP (i.e.,  $k^* \in K^*$ ) with the lowest estimated location error for this group. In summary, the proposed user grouping algorithm is given in Algorithm 1.

**Algorithm 1** LiDAL-assisted RLNC-NOMA User Grouping

- 1: Initialize  $N \leftarrow$  OWC users
- 2: Initialize  $K \leftarrow$  Optical APs
- 3: **for**  $i \leftarrow 1, N$  **do**
- 4:   Compute the Euclidean distance  $f_i(k), \forall k \in K$  of the location of user  $i$  on the communication plane to all optical APs.
- 5:   Find the feasible sets of adjacent APs  $K^* \subset K$  that have the minimum Euclidean distance  $f_i(k)$  to user  $i$ .
- 6: **end for**
- 7: **for**  $k \leftarrow 1, K^*$  **do**
- 8:   Sort all the potential users  $M^k$  of optical AP  $k$  according to their location CRLB error estimation  $B_k^L(X_m) \forall m \in M^k$ .
- 9:   Divide the  $M^k$  users into two classes (i.e., Class I and Class II).
- 10:   **for**  $m \leftarrow 1, M_j^k, j = \{1, 2\}$  **do**
- 11:     Sort each class  $j$  users  $M_j^k$  according to their access distance to optical AP  $k$ .  

$$\Lambda_1^k \leq \Lambda_2^k \leq \dots \leq \Lambda_m^k \leq \Lambda_{m+1}^k \leq \dots \leq \Lambda_{M_j^k}^k$$
- 12:   **end for**
- 13:   Pair the all  $M^k$  users in both classes according to D-NLUPA pairing method [41].
- 14: **end for**
- 15: Assign the group of paired users to the AP  $k^* \in K^*$  that have the minimum average estimated location errors of the users in this group.
- 16: Ensure no duplicate users in the group assigned to the optical AP  $k^*$ .

IV. SIMULATION AND PERFORMANCE EVALUATION

A. Simulation Setup

In Fig.1, eight RGB-LD APs are used to serve communication users and estimate their locations within the formed overlapped optical footprints that meet the required illumination and eye safety standards (i.e.,  $K = 8$ ). We considered a realistic indoor environment with reflections generated by user skin color, cloth materials (i.e., cotton, polyester), indoor surfaces and objects (i.e., walls, furniture, door, and ceiling). The reflections of these elements can be represented as a combination of diffuse and specular reflectors. In this work, a stochastic process (i.e., normalized Gaussian distribution) of diffuse reflectivity is assumed and referred to by the factor  $\rho$  in equations (10) and (11) to model the reflections of target users, objects, and surfaces that dominate the reflected light beams in the considered indoor space [33]. Moreover, Lambertian first- and second-order diffuse light reflections are measured and the impulse response of reflected optical pluses is collected from the effective cross section area  $d_A$  of an arbitrary target user or object within the proposed indoor environment. A 300 MHz receiver bandwidth and zero forcing equalizer (ZFE) are used for LiDAL receivers to meet the proposed minimum LiDAL resolution  $\Delta R = 0.3m$ . Therefore, 378 locations on the communication plane are considered to represent the possible user locations that the MIMO-LiDAL system can detect a

user and estimate its location within the indoor environment studied. Note that, the same receiver responsivity factor  $\mathfrak{R}$  is assumed for both the user receiver and the LiDAL system receivers in terms of thermal and shot noises. Additionally, we assume an identical vertical height difference  $\eta$  for both the PD of the user communication receiver  $A_{PD}$  and the user detection cross section  $d_A$  for localization (refer to equations (11) and (10)). The transmitted packets are encoded in GF(2<sup>8</sup>) and modulated using the non-return-to-zero on-off keying (NRZ-OOK) modulation scheme. For SIC, the received superimposed optical signals are estimated and detected using the maximum likelihood method. The spare RLNC encoding / decoding scheme [35] is used to generate fixed-length coded packets along with the randomly generated coding vectors to be decoded over the estimated erasure channel. The remaining parameters of both the RLNC-NOMA and MIMO-LiDAL systems are listed in Table I.

TABLE I  
SYSTEM SETUP PARAMETERS

Parameters	Configurations
Room dimensions ( $x \times y \times z$ )	$4 \times 8 \times 3 \text{ m}^3$ [38]
Finished-wood,walls, floor and ceiling reflectivity factors,	0.55 ,0.8, 0.3, 0.8 [38]
Total transmitted optical power, $P_t$	18 W [38]
Transmitter semi-angle at half power beamwidth, $\Phi_{1/2}$	75° [38]
APs locations (x,y,z)	(1,1,3),(1,3,3),(1,5,3),(1,7,3), (3,1,3),(3,3,3),(3,5,3),(3,7,3) [38]
Azimuth	0°
Elevation	90°
Optical receiver PD area, $A_{PD}$	20mm <sup>2</sup> [38]
PD filter gain, $T_f(\psi)$	1 [38]
Optical concentrator gain, $g_c(\psi)$	3.77
PD responsivity, $\mathfrak{R}$	0.4 A/W [38]
Concentrator reflective index, $n$	1.7 [38]
<b>MIMO-LiDAL system</b>	
LiDAL receiver FOV, $\Psi^L$	54°
Transmitted pulse width	2 ns [38]
LiDAL receiver time slot	2 ns [38]
LiDAL receiver bandwidth, $B_w^L$	300 MHz [38]
The optical footprint diameter	2.6 m
The maximum optical footprints overlap	0.6 m
Time bin duration	0.01 ns [38]
<b>RLNC-NOMA system</b>	
User cross section height, $h'$	0.8 m
User receiver FOV, $\Psi_c$	40° [9]
Elevation	90°
Azimuth	0°
User receiver bandwidth, $B_w$	20 MHz [9]
RLNC generation size, $f$	3 packets [16]
Minimum NOMA user throughput, $\zeta$	0.5 bits/s. $H z^{-1}$ [9]

B. RLNC-NOMA Decoding Success Probability

Fig.8 illustrates the overall success probability of the proposed RLNC-based NOMA and OMA schemes in relation to the power allocation coefficient  $\alpha$ . This coefficient is assigned to the user with the lowest estimated location order among a group of four sorted users according to the proposed LiDAL-NOMA grouping scheme (see Algorithm 1). These users are served by a single optical AP  $k \in K$ . The analysis of the

depicted results shows that both RLNC-NOMA and RLNC-OMA provide a higher overall packet success probability compared to traditional NOMA and OMA schemes for all designated group users. This can be interpreted as using RLNC

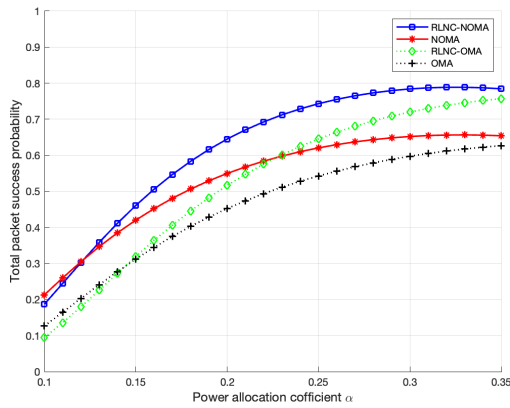


Fig. 8. RLNC-NOMA and RLNC-OMA packet success probability versus the power allocation coefficient  $\alpha$ .

helps make transmission schemes more resistant in high-noise scenarios, which is expected due to the fact that the original packets are superposed into coded packets that reduce error.

Furthermore, RLNC-OMA outperforms conventional NOMA when the power allocation coefficient  $\alpha$  assigned to the user of the lowest location order increases, as this scheme assigns an exclusive frequency or time slot to each user to avoid interference among them. However, RLNC-NOMA provides higher packet success probability compared to RLNC-OMA, especially in scenarios where the power is carefully allocated among the users of the same group under NOMA principles.

### C. MIMO-LiDAL Localization Probability

We optimized the probability of localization of the proposed MIMO-LiDAL system in the considered indoor environment modeled similar to [33]. We Focus on two parameters of the LiDAL receiver design, the LiDAL receiver FOV angle  $\Psi^L$ , and the TOA location estimator in the MIMO-LiDAL system model. However, we maintain the same system configurations such as the generation of optical pulses, transceiver locations, optical detection parameters, and the CCM detection scheme as defined in Table 9 [33]. For the FOV angle of the LiDAL receiver, an exhaustive search is applied to find the optimal angle  $\Psi^L = 54^\circ$  for the optical signals received in the formed and overlapped optical footprints while reducing the effect of the reflections of the first and second order signals generated by indoor objects and surfaces. For the TOA location estimator, the biconjugate gradient method [42] is used to numerically approximate the quadratic terms in (17). The results in Fig.9 show that the probability of localization is improved on average by 23% by the proposed design of the MIMO-LiDAL system in both dimensions (x,y) of the indoor communication plane compared to the baseline design proposed in [33].

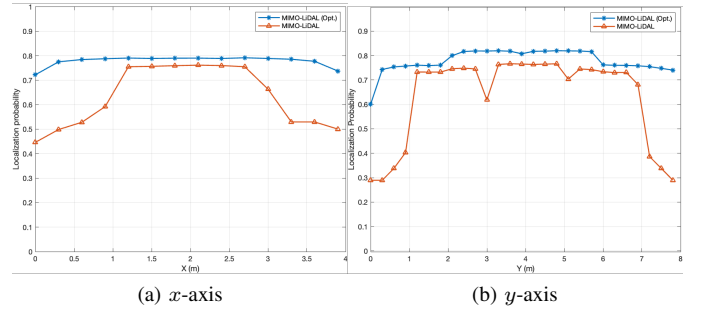


Fig. 9. PDF of MIMO-LiDAL localization on  $x$  and  $y$  -axis, respectively.

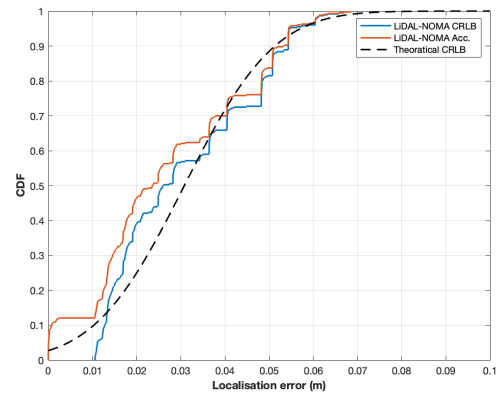


Fig. 10. CDF of MIMO-LiDAL Localization CRLB vs accuracy for the proposed indoor OWC system.

### D. MIMO-LiDAL Localization CRLB and Accuracy

We numerically evaluated the CRLB derived for the proposed MIMO-LiDAL system, as depicted in Fig.10 for the indoor environment considered. The results highlight the distribution of the CRLB error estimations of the localization of the MIMO-LiDAL system across the communication plane while maintaining the assumption of the minimum detection resolution constraint  $\Delta R = 0.3m$ . Furthermore, we computed the noise covariance matrix ( $\mathbb{Q}$ ) in (41) that consisted of ambient background noise that includes from the walls and surfaces of oblique objects (i.e., doors and tables), receiver noise components, and interfered LOS optical pulses (i.e., detection pulses within overlapped bistatic subsystems).

To validate the results of the CRLB analysis, we compared it to the localization accuracy of the MIMO-LiDAL system at all potential user locations on the communication plane, as demonstrated in Fig.10. The CDF graph depicts a close correlation between the CRLB bound and the localization accuracy of the proposed MIMO-LiDAL system, highlighting that the accuracy for 95% of user locations is under 6 cm. Furthermore, the findings indicate that the CRLB function is suitable as a distance-based parameter to approximate the state of the user channel.

### E. LiDAL-assisted User Grouping

In this section, we evaluate the proposed LiDAL-assisted user grouping algorithm using the simulated indoor environ-

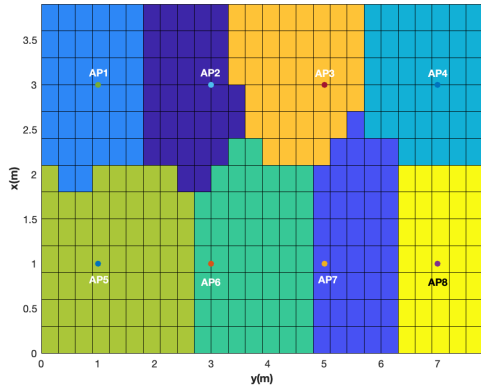


Fig. 11. The associated OWC user locations to APs using the LiDAL-assisted user grouping scheme.

ment of the proposed RLNC-NOMA OWC system. Initially, we determined the possible locations in which an arbitrary user  $i$  can be detected and localized on the communication plane using the proposed MIMO-LiDAL system. As a result, we found that 378 possible estimated locations satisfy the minimum localization resolution condition  $\Delta R = 0.3$  on the communication plane in the proposed indoor environment. Second, we applied the user grouping scheme in Algorithm 1 on these possible locations to dynamically divide them into groups and assign each formed group to one of the system optical APs (i.e.,  $K = 8$ ). The distribution of these locations within the generated groups ranges from 10.32% to 15.87%. These formed groups satisfy the three necessary conditions of the proposed algorithm: the minimum Euclidean distance between an arbitrary user  $i$  in these 378 possible locations and the optical APs of the system, the access distances (i.e., the LOS distance between the receiver of user  $i$  and the potential APs  $K^*$ ) sorted in ascending order and assigned to optical AP  $k^*$  with the lowest average in estimated user location errors. Fig.11 depicts the locations served by each optical AP  $k$  using our proposed grouping algorithm.

#### F. LiDAL-assisted RLNC-NOMA sum rate

Gain ratio power allocation (GRPA) [43] is applied as a baseline power allocation scheme that assigns the optical AP  $k$  power ratio to the user  $i$  based on his imperfect CSI channel coefficient (i.e.,  $h_i^*$ ), the approximated CSI channel coefficient (i.e.,  $h_i^* + \Delta h_i^*$ ) as in (8) and both are compared to his perfect CSI channel coefficient (i.e.,  $h_i$ ) at all possible locations within a designated group  $k$ . In Fig.12, the empirical CDF graphs depicted reflect the sum rate of possible locations in which user  $i$  can be located under the MIMO-LiDAL minimum resolution constraint and within the LiDAL-based groups formed as shown in Fig.11. The sum rate metric is selected to analyze how the user location information exploited affects the estimation of the CSI channel coefficients. It also evaluates the overall performance of the RLNC-NOMA system using the proposed LiDAL-assisted grouping scheme in the considered indoor environment. The graphs reflect that the

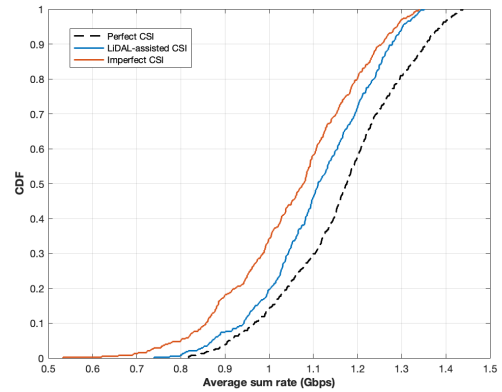


Fig. 12. LiDAL-assisted RLNC-NOMA achievable sum rate.

use of location-based information provided by the MIMO-LiDAL system significantly improves the estimation of the CSI channel coefficients, showing a performance comparable to the perfect CSI channel coefficients in terms of the sum rate. Here, the power ratios are assigned to the sorted user locations within each group relative to the highest estimated CSI channel coefficient w/o LiDAL assistance in that group. However, we observed that the sum rate achieved is not optimal under the selected power allocation scheme (i.e. GRPA) compared to the perfect CSI scenario.

#### V. CONCLUSION

In this work, we proposed an integration of the MIMO-LiDAL system into a RLNC-NOMA-based OWC system. We first introduced a RLNC-NOMA scheme to improve NOMA performance in terms of decoding success probability and system capacity. Then, a MIMO-LiDAL system is defined for localization and better CSI estimation in realistic indoor scenarios. We derived the CRLB of the proposed system model as an unbiased location error estimator and developed a suboptimal user grouping scheme in a given indoor environment. The simulation results highlight that the RLNC-NOMA approach outperformed conventional NOMA and OMA schemes in terms of packet decoding reliability. In addition, location-based information provided by the MIMO-LiDAL system significantly improved the estimation of CSI channel coefficients, achieving a performance comparable to the systems with perfect CSI coefficients. However, optimizing power allocation within the proposed system is still an area that needs further investigation.

#### ACKNOWLEDGMENT

The authors would like to acknowledge funding from the Engineering and Physical Sciences Research Council (EPSRC) TOWS (EP/S016570/2) and TITAN (EP/X04047X/2) projects. For the purpose of open access, the authors have applied a Creative Commons Attribution (CC BY) license to any Author Accepted Manuscript version arising. All data are provided in full in the results section of this article.

## REFERENCES

- [1] O. Alsulami, A. T. Hussein, M. T. Alresheedi, and J. M. H. Elmirghani, "Optical Wireless Communication Systems, A Survey," p. 22.
- [2] A. A. Qidan, M. Morales-Cespedes, A. Garcia-Armad, and J. M. H. Elmirghani, "Resource allocation in user-centric optical wireless cellular networks based on blind interference alignment," *Journal of Lightwave Technology*, vol. 39, no. 21, pp. 6695–6711, 2021.
- [3] A. A. Qidan, M. Morales-Cespedes, and A. Garcia-Armad, "Load balancing in hybrid vlc and rf networks based on blind interference alignment," *IEEE Access*, vol. 8, pp. 72 512–72 527, 2020.
- [4] P. H. Pathak, X. Feng, P. Hu, and P. Mohapatra, "Visible Light Communication, Networking, and Sensing: A Survey, Potential and Challenges," *IEEE Communications Surveys & Tutorials*, vol. 17, pp. 2047–2077, 2015.
- [5] A. A. Qidan, M. Morales-Cespedes, and A. Garcia-Armada, "User-centric blind interference alignment design for visible light communications," *IEEE Access*, vol. 7, pp. 21 220–21 234, 2019.
- [6] A. A. Qidan, M. Morales-Cespedes, A. Garcia-Armad, and J. M. H. Elmirghani, "User-centric cell formation for blind interference alignment in optical wireless networks," in *ICC 2021 - IEEE International Conference on Communications*, 2021, pp. 1–7.
- [7] S. Feng, R. Zhang, W. Xu, and L. Hanzo, "Multiple Access Design for Ultra-Dense VLC Networks: Orthogonal vs Non-Orthogonal," *IEEE Transactions on Communications*, vol. 67, pp. 2218–2232, Mar. 2019.
- [8] X. Zhang, Q. Gao, C. Gong, and Z. Xu, "User Grouping and Power Allocation for NOMA Visible Light Communication Multi-Cell Networks," *IEEE Communications Letters*, vol. 21, pp. 777–780, Apr. 2017.
- [9] L. Yin, X. Wu, and H. Haas, "On the performance of non-orthogonal multiple access in visible light communication," in *2015 IEEE 26th Annual International Symposium on Personal, Indoor, and Mobile Radio Communications (PIMRC)*, Aug. 2015, pp. 1354–1359.
- [10] H. Marshoud, P. C. Sofotasios, S. Muhaidat, G. K. Karagiannidis, and B. S. Sharif, "On the Performance of Visible Light Communication Systems With Non-Orthogonal Multiple Access," *IEEE Transactions on Wireless Communications*, vol. 16, pp. 6350–6364, Oct. 2017.
- [11] T. Ho, M. Medard, R. Koetter, D. Karger, M. Effros, J. Shi, and B. Leong, "A Random Linear Network Coding Approach to Multicast," *IEEE Transactions on Information Theory*, vol. 52, pp. 4413–4430, Oct. 2006.
- [12] H.-T. Lin, Y.-Y. Lin, W.-S. Yan, and F.-B. Hsieh, "Efficient Frame Aggregation Transmission Using Random Linear Network Coding," *IEEE Wireless Communications Letters*, vol. 3, pp. 629–632, Dec. 2014.
- [13] Y. Hong, L.-K. Chen, and X. Guan, "Adaptive physical-layer network coding over visible light communications," in *2017 Optical Fiber Communications Conference and Exhibition (OFC)*, Mar. 2017, pp. 1–3.
- [14] Z.-Y. Wang, H.-Y. Yu, and D.-M. Wang, "Energy-Efficient Network Coding Scheme for Two-Way Relay Visible Light Communications," in *2018 IEEE 18th International Conference on Communication Technology (ICCT)*, Oct. 2018, pp. 310–315.
- [15] Y. Hong, L.-K. Chen, and J. Zhao, "Channel-Aware Adaptive Physical-Layer Network Coding Over Relay-Assisted OFDM-VLC Networks," *Journal of Lightwave Technology*, vol. 38, pp. 1168–1177, Mar. 2020.
- [16] S. Park and D.-H. Cho, "Random Linear Network Coding Based on Non-Orthogonal Multiple Access in Wireless Networks," *IEEE Communications Letters*, vol. 19, pp. 1273–1276, Jul. 2015.
- [17] A. A. Hassan, A. Adnan Qidan, T. Elgorashi, and J. Elmirghani, "Random Linear Network Coding for Non-Orthogonal Multiple Access in Multicast Optical Wireless Systems," in *2023 23rd International Conference on Transparent Optical Networks (ICTON)*, Jul. 2023, pp. 1–5.
- [18] Z. Yang, Z. Ding, P. Fan, and G. K. Karagiannidis, "On the Performance of Non-orthogonal Multiple Access Systems With Partial Channel Information," *IEEE Transactions on Communications*, vol. 64, pp. 654–667, Feb. 2016.
- [19] S. A. R. Zekavat, S. Kansal, and A. H. Levesque, "Wireless Positioning Systems: Location, Application, and Comparison," in *Handbook of Position Location*. John Wiley & Sons, Ltd, 2011, pp. 3–23.
- [20] B. Zhou, A. Liu, and H. C. So, "Visible Light Communication-Enabled Simultaneous Position and Orientation Detection for Harnessing Multipath Interference and Random Fading," *IEEE Transactions on Intelligent Transportation Systems*, pp. 1–15, 2023.
- [21] Y. Chen, W. Guan, J. Li, and H. Song, "Indoor Real-Time 3-D Visible Light Positioning System Using Fingerprinting and Extreme Learning Machine," *IEEE Access*, vol. 8, pp. 13 875–13 886, 2020.
- [22] J. Luo, L. Fan, and H. Li, "Indoor Positioning Systems Based on Visible Light Communication: State of the Art," *IEEE Communications Surveys & Tutorials*, vol. 19, pp. 2871–2893, 2017.
- [23] Y. S. Eroglu, I. Guvenc, N. Pala, and M. Yuksel, "AOA-based localization and tracking in multi-element VLC systems," in *2015 IEEE 16th Annual Wireless and Microwave Technology Conference (WAMICON)*, Apr. 2015, pp. 1–5.
- [24] M. F. Keskin, S. Gezici, and O. Arikan, "Direct and Two-Step Positioning in Visible Light Systems," *IEEE Transactions on Communications*, vol. 66, pp. 239–254, Jan. 2018.
- [25] S.-H. Yang, E.-M. Jung, and S.-K. Han, "Indoor Location Estimation Based on LED Visible Light Communication Using Multiple Optical Receivers," *IEEE Communications Letters*, vol. 17, pp. 1834–1837, 2013.
- [26] W. Guan, L. Huang, S. Wen, Z. Yan, W. Liang, C. Yang, and Z. Liu, "Robot Localization and Navigation Using Visible Light Positioning and SLAM Fusion," *Journal of Lightwave Technology*, vol. 39, pp. 7040–7051, Nov. 2021.
- [27] C. L. P. Chen, H. Li, Y. Wei, T. Xia, and Y. Y. Tang, "A Local Contrast Method for Small Infrared Target Detection," *IEEE Transactions on Geoscience and Remote Sensing*, vol. 52, pp. 574–581, Jan. 2014.
- [28] J. Nissinen and J. Kostamovaara, "A High Repetition Rate CMOS Driver for High-Energy Sub-ns Laser Pulse Generation in SPAD-Based Time-of-Flight Range Finding," *IEEE Sensors Journal*, vol. 16, pp. 1628–1633, Mar. 2016.
- [29] Y. Wen, F. Yang, J. Song, and Z. Han, "Pulse Sequence Sensing and Pulse Position Modulation for Optical Integrated Sensing and Communication," *IEEE Communications Letters*, vol. 27, pp. 1525–1529, Jun. 2023.
- [30] H. Hawkins, C. Xu, L.-L. Yang, and L. Hanzo, "IM-OFDM ISAC Outperforms OFDM ISAC By Combining Multiple Sensing Observations," *IEEE Open Journal of Vehicular Technology*, pp. 1–19, 2024.
- [31] T. Q. Wang, Y. Sekercioglu, A. Neild, and J. Armstrong, "Position Accuracy of Time-of-Arrival Based Ranging Using Visible Light With Application in Indoor Localization Systems," *Journal of Lightwave Technology*, vol. 31, pp. 3302–3308, 2013.
- [32] H. Lv, L. Feng, A. Yang, P. Guo, H. Huang, and S. Chen, "High Accuracy VLC Indoor Positioning System With Differential Detection," *IEEE Photonics Journal*, vol. 9, pp. 1–13, 2017.
- [33] A. A. Al-Hameed, S. H. Younus, A. T. Hussein, M. T. Alresheedi, and J. M. H. Elmirghani, "LiDAL: Light Detection and Localization," *IEEE Access*, vol. 7, pp. 85 645–85 687, 2019.
- [34] S. Ma, R. Yang, C. Du, H. Li, Y. Wu, N. Al-Dhahir, and S. Li, "Robust Power Allocation for Integrated Visible Light Positioning and Communication Networks," *IEEE Transactions on Communications*, vol. 71, pp. 4764–4777, Aug. 2023.
- [35] M. Pedersen, J. Heide, and F. Fitzek, "Kodo: An Open and Research Oriented Network Coding Library," Jan. 2011, pp. 145–152.
- [36] A. S. Khan, "Characterisation and performance analysis of random linear network coding for reliable and secure communication," phd, Lancaster University, 2018.
- [37] A. L. Jones, I. Chatzigeorgiou, and A. Tassi, "Binary systematic network coding for progressive packet decoding," in *2015 IEEE International Conference on Communications (ICC)*, Jun. 2015, pp. 4499–4504.
- [38] A. A. Al-Hameed, S. H. Younus, A. T. Hussein, M. T. Alresheedi, and J. M. H. Elmirghani, "Artificial Neural Network for LiDAL Systems," *IEEE Access*, vol. 7, pp. 109 427–109 438, 2019.
- [39] E. Tsimbalo, A. Tassi, and R. J. Piechocki, "Reliability of Multicast Under Random Linear Network Coding," *IEEE Transactions on Communications*, vol. 66, pp. 2547–2559, Jun. 2018.
- [40] H. Godrich, A. M. Haimovich, and R. S. Blum, "Target Localization Accuracy Gain in MIMO Radar-Based Systems," *IEEE Transactions on Information Theory*, vol. 56, pp. 2783–2803, Jun. 2010.
- [41] S. M. R. Islam, M. Zeng, O. A. Dobre, and K.-S. Kwak, "Resource Allocation for Downlink NOMA Systems: Key Techniques and Open Issues," *IEEE Wireless Communications*, vol. 25, pp. 40–47, Apr. 2018.
- [42] B. Zhou, A. Liu, and V. Lau, "Joint User Location and Orientation Estimation for Visible Light Communication Systems With Unknown Power Emission," *IEEE Transactions on Wireless Communications*, vol. 18, pp. 5181–5195, Nov. 2019.
- [43] H. Marshoud, V. M. Kapinas, G. K. Karagiannidis, and S. Muhaidat, "Non-Orthogonal Multiple Access for Visible Light Communications," *IEEE Photonics Technology Letters*, vol. 28, pp. 51–54, Jan. 2016.